Nanosilicon electrodes for lithium-ion batteries: Interfacial mechanisms studied by hard and soft X-ray photoelectron spectroscopy

Bertrand Philippe, Rémi Dedryvère, Joachim Allouche, Frederik Lindgren, Mihaela Gorgoi, Håkan Rensmo, Danielle Gonbeau, Kristina Edström

Nano-silicon electrodes for lithium-ion batteries: interfacial mechanisms studied by hard and soft X-ray Photoelectron Spectroscopy

Bertrand Philippe [1,2,5], Rémi Dedryvère [1,5,*], Joachim Allouche [1],
Fredrik Lindgren [2,5], Mihaela Gorgoi [3], Håkan Rensmo [4,5], Danielle Gonbeau [1,5],
Kristina Edström [2,5,*]

[1] IPREM/ECP (UMR 5254), University of Pau, Hélioparc, 2 av. Pierre Angot, 64053 Pau cedex 9, France
[2] Dept. of Materials Chemistry, Ångström Lab., Uppsala University, Box 538, SE-75121 Uppsala, Sweden
[3] Helmholz-Zentrum Berlin, 12489 Berlin, Germany
[4] Dept. of Physics, Uppsala University, P.O. Box 530, SE-75121, Uppsala, Sweden
[5] Alistore - European Research Institute, 33 rue Saint-Leu, 80039 Amiens cedex, France

Abstract

Largely based on its very high rechargeable capacity, silicon appears as an ideal candidate for the next generation of negative electrodes for Li-ion batteries. However, a crucial problem with silicon is the large volume expansion undergone upon alloying with lithium, which results in stability problems. Means to avoid such problems is largely linked to the understanding of the interfacial chemistry during charging/discharging. This is especially of great importance when using nanometric silicon particles. In this work, the interfacial mechanisms (reaction of surface oxide, Li-Si alloying process, passivation layer formation) accompanying lithium insertion/extraction into Si/C/CMC composite electrodes have been scrutinized by X-ray photoelectron spectroscopy (XPS). A thorough non-destructive depth-resolved analysis was carried out by using both soft X-rays (100-800 eV) and hard X-rays (2000-7000 eV) from two different synchrotron facilities compared with in-house XPS (1487 eV). The unique combination utilizing hard and soft x-ray photoelectron spectroscopy accompanied with variation of the analysis depth allowed us to access interfacial phase transitions at the surface of silicon particles as well as the composition and thickness of the SEI (electrode/electrolyte interface layer).

Keywords : Lithium-ion batteries, silicon, alloy, SEI, XPS, PES, synchrotron

* corresponding authors (remi.dedryvere@univ-pau.fr, kristina.edstrom@kemi.uu.se)

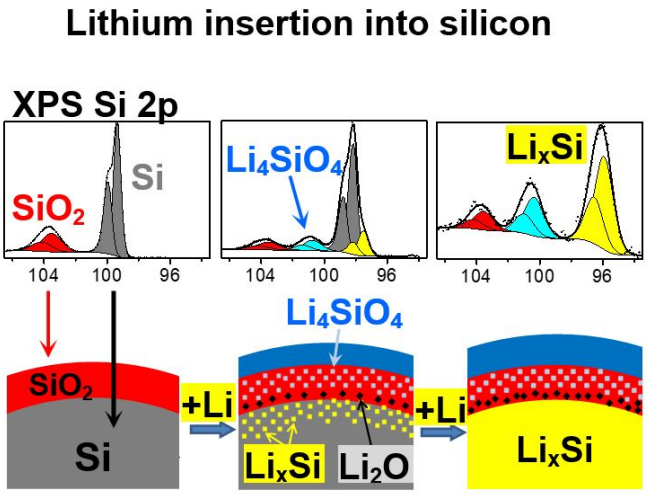

1. Introduction

The development of the lithium-ion (Li-ion) battery technology has made the tremendous development of portable electronics industry possible. Most commercial lithium-ion batteries use carbonaceous materials as negative electrode. Today the research of new electrode materials for Li-ion batteries is motivated by an increasing need for efficient energy storage systems for renewable energies and urban transportation [1,2,3,4]. Indeed, new emerging applications require higher performances in terms of rechargeable capacity, energy density, power and safety. Alternative materials must also be inexpensive and environmentally friendly. Metals and semimetals that can electrochemically form alloys with lithium are an interesting alternative, because they lead to very high rechargeable capacity values. Silicon can theoretically alloy with 4.4 Li atoms per Si atom ($Li_{22}Si_5$) [5,6,7]. Actually, the fully lithiated state at room temperature is $Li_{15}Si_4$ which corresponds to a maximum capacity of 3578 mAh/g [8], a very high value with respect to ~330 mAh/g for graphite. Besides, silicon is a light and abundant element, so it appears as an ideal candidate for the next generation of negative electrodes. A crucial problem is the large volume changes undergone by silicon upon

alloying and de-alloying with lithium (~300 % volume expansion upon lithiation), which results in strong mechanical strains and subsequent loss of electrical contacts between silicon, the conductive matrix and the current collector [9,10]. Several strategies have been considered to reduce this volume change and improve the stability of the silicon electrodes, either by using nanosized particles that better sustain the mechanical strains, or by using specific cycling conditions of the battery (current rates, cut-off voltages, pre-cycling) [11,12,13]. A significant improvement was achieved by using sodium carboxymethyl cellulose binder (CMC) that facilitates a networking process of the conductive carbon additive and Si particles during the composite electrode preparation [11,14,15].

However, despite these improvements cycling performances of silicon electrodes still remain unsatisfactory for a use in practical Li-ion batteries. Particularly, some limitations are due to electrode/electrolyte interfaces. Therefore it is necessary to better understand this interface reactivity. Compared to interface phenomena on carbonaceous electrodes that have been extensively studied for many years [16], much less research attention has been devoted to interfacial mechanisms onto silicon negative electrodes. This is especially important for nanometric silicon particles due to their high specific surface areas, since the formation of the Solid Electrolyte Interphase (SEI) layer is recognized as one of the key points for Li-ion battery performance and safety, which are strongly dependent on the stabilization of electrode/electrolyte interfacial reactions.

For silicon electrodes (like for Sn- or Sb-based intermetallic electrodes) the surface of the active material undergoes a continuous reconstruction due to the considerable volume changes. The SEI is thus supposed to follow the changes of the surface and its continuous formation may consume a large amount of lithium and electrolyte components, and consequently it may contribute to the irreversible capacity [17]. In a previous paper, Chan *et al.* [18] analyzed the

composition and morphology of the SEI formed on silicon nanowires by X-ray photoelectron spectroscopy (XPS) and scanning electron microscopy (SEM). The morphology of the SEI was reported to be voltage dependent with a thicker SEI at low potential and a partial dissolution and cracking during the delithiation. After the first lithiation below 0.1 V *vs.* Li^+/Li the SEI was found to be thicker than the XPS analysis depth (~10 nm), and consequently the Si 2p signal was not observable. In this case, the Si 2p signal was revealed after Ar^+ ion etching to remove the SEI. On the other hand, the composition of the SEI was consistent with that observed on graphite electrodes. Lee *et al.* [19] analyzed the SEI formation on amorphous silicon thin film electrodes step by step during the first cycle. They showed from electrochemical impedance spectroscopy (EIS) that the native surface layer (SiO_2 and Si-OH) covering the Si electrode is destroyed at the beginning of the first discharge. However, the destruction of this native oxide as well as the mechanisms occurring at the Si surface could not be directly observed by XPS as Si 2p core peaks are not observable when the potential is lower than 0.25 V due to the SEI thickness.

In the present work, we followed the evolution of different materials of importance for describing the interfacial mechanisms (reaction of the surface oxide, Li-Si alloying process, passivation layer formation) occurring upon the first lithiation/delithiation cycle of Si/C/CMC composite electrodes in Li/Si electrochemical cells. This has been accomplished by Photoelectron Spectroscopy (PES). In our approach we have developed non-destructive depth-resolved analysis by varying the energy of the X-ray photons, instead of using destructive argon ion sputtering. To this aim, the electrodes were studied by both soft X-ray PES (photon energy $h\nu$ = 100-800 eV) and hard X-ray photoelectron spectroscopy (HAXPES, $h\nu$ = 2000-7000 eV) at two different synchrotron facilities (MaxIV Laboratory, Lund,

Sweden; and Bessy II, Helmholtz Centre, Berlin, Germany) as well as by the use of in-house XPS (Al Kα = 1486.6 eV).

2. Experimental details

2.1. Electrochemical cycling:

Silicon electrodes were prepared using 80 % of crystalline silicon powder (~50 nm), Alfa Aesar), 12 % of conductive carbon black (SuperP, Erachem Comilog) and 8 % of sodium carboxymethyl cellulose (CMC, M_w = 700.000, DS = 0.9, Sigma Aldrich) as binder. A water-ethanol solution (EtOH/H_2O, 70/30) was used as solvent for the slurry preparation. The slurry was mixed in a Retsch planetary mill for 60 min, then deposited on a 0.02 mm thick copper foil and dried at 60°C for 12h in an oven to obtain a ~12-13 µm coating thickness. Circular electrodes (2 cm diameter) were punched out and dried for 8h at 120°C in a vacuum oven inside the argon glovebox (O_2 < 3 ppm, H_2O < 1 ppm).

Electrochemical cells were assembled by stacking the Si/C/CMC composite electrode (working electrode), a lithium foil (counter and reference electrode), and a polymer separator soaked with the electrolyte ($LiPF_6$ at 1 mol/L dissolved in ethylene carbonate/ diethyl carbonate with ratio EC/DEC 2/1). Karl Fischer titration showed the water content to be below 10 ppm (the detection limit of the instrument). This assembly was hermetically vacuum-sealed in a polyethylene-coated aluminum bag with attached nickel tabs as current collectors. Electrochemical discharge and charge were carried out with a Digatron BTS-600 testing apparatus under galvanostatic mode with a current of 150 mA/g of silicon (C/6 rate, which means that 1 mole of Li reacts with 1 mole of Si in 6 hours). The cells were cycled between 0.01 V and 0.9 V (*vs.* Li^+/Li) and stopped at various potential values, with a break of 5 min between discharge and charge. After cycling the voltage was fixed for one hour to

allow relaxation of the cell. The cell was then disconnected and the current connectors were protected with an adhesive tape to avoid short-circuit during transportation.

Before each characterization, the silicon electrode was carefully separated from the rest of the battery component in an argon glovebox and washed with dimethyl carbonate (DMC) solvent in three successive baths to remove the electrolyte. For each bath, the electrode was put into 2mL of ultralow water content DMC in a clean and dry aluminum container, maintaining a mild manual agitation during 1 min. Then the electrode was removed from the container and put into the following. After the third bath, the electrode was dried.

2.2. Lithium silicates synthesis:

Lithium metasilicate (Li_2SiO_3) and lithium orthosilicate (Li_4SiO_4) were synthesized by *(i)* sol gel (Li_2SiO_3 and Li_4SiO_4) and *(ii)* precipitation (Li_4SiO_4) methods. *(i)* The sol-gel process used in this work largely follows the procedure previously reported by Zhang *et al.* [20]. For each compound, tetraethyl orthosilicate (TEOS, Aldrich) and lithium ethoxide (1 mol/L solution in ethanol, Aldrich) precursors were mixed with the targeted Li/Si molar ratios. The solution was stirred with a magnetic stirrer for 40 min at room temperature. During this period the reaction vessel was closed with a plastic film. A mixture of distilled deionized water and ethanol (33 vol.% water) was then added drop wise to effect hydrolysis. After a few minutes, condensation of TEOS occurred and the solution has become opaque viscous. The solution was allowed to stand overnight at room temperature with the reaction vessel covered, and then the remaining water and ethanol were evaporated in an oven at 50°C until a dry powder was obtained. The dry powder was then calcined in an air furnace at 900°C for 4h. *(ii)* For precipitation synthesis, the process used by Pfeiffer *et al.* [21] was used. Amorphous SiO_2 was suspended in water as a first step. An aqueous solution of LiOH (Aldrich) was then slowly

added to the suspension to obtain a Li/Si molar ratio of 4. The mixture was stirred and heated at 70°C until dried, and then the powder was calcined at 900°C for 4h.

2.3. X-ray photoelectron spectroscopy:

For all XPS experiments, careful precautions were taken in order to avoid moisture/air exposure of samples during transfer. Samples were transferred to the spectrometer either directly from the argon glovebox via a glass window and a transfer chamber (in-house), or with the help of a stainless steel sample holder hermetically encapsulated in the glovebox and opened in the vacuum preparation chamber (at the synchrotron). The binding energy scale was calibrated from the hydrocarbon C 1s peak at 285.0 eV.

2.3.1. In-house XPS: Measurements were carried out with a Kratos Axis Ultra spectrometer, using a focused monochromatized Al Kα radiation (hν = 1486.6 eV). For the Ag $3d_{5/2}$ line the full width at half maximum (FWHM) was 0.58 eV under the recording conditions. The analyzed area of the samples was 300 × 700 μm^2. The pressure in the analysis chamber was around 5.10^{-9} mbar. Core peaks were analyzed using a nonlinear Shirley-type background [22]. The peak positions and areas were optimized by a weighted least-square fitting method using 70 % Gaussian, 30 % Lorentzian lineshapes. Quantification was performed on the basis of Scofield's relative sensitivity factors [23].

2.3.2. Soft X-ray PES: Measurements were carried out at the MaxIV Laboratory synchrotron facility (I-411 beamline, National Synchrotron Radiation Laboratory, Lund, Sweden), where the usable photon energies range from 50 to 1500 eV. Photons were monochromatized by a Zeiss SX-700 plan grating monochromator. The photoelectron kinetic energies (K.E.) were measured using a Scienta R4000 WAL analyzer. Due to low photon energies, measurements were conducted in such a way that the same photoelectron K.E. was

used for all probe elements. In this way, the selected K.E. 130 eV is obtained with hν = 230 eV for Si 2p spectra, hν = 410 eV for C 1s spectra, hν = 660 eV for O 1s spectra, hν = 810 eV for F 1s spectra, corresponding to the same analysis depth for all spectra. No charge neutralizer was used during the measurements. The pressure in the analysis chamber was about 10^{-8} mbar.

2.3.3. Hard X-ray PES: Measurements were carried out at Bessy II synchrotron facility (HIKE end station, KMC-1 beamline, Helmholtz Zentrum, Berlin, Germany [24]), where the usable photon energies range from 2000 to 10000 eV. Fixed excitation energies were used, 2300 and 6900 eV (first and third order lights from the Si(111) crystal in the double-crystal monochromator). For such high photon energies we could assume the same probing depth for the core levels probed in the present investigation, and so it was not necessary to fix the same K.E. in this case. The analyser was a Scienta R4000 optimized for high kinetic energies up to 10 keV. No charge neutralizer was used and the pressure was around 10^{-8} mbar.

3. Results and discussion

Figure 1 shows Si 2p XPS spectra of the pristine silicon electrode obtained with various photon energies (hν). Low energies (100-800 eV) correspond to soft X-ray PES (MaxIV Lab. synchrotron), middle energy (1486.6 eV) corresponds to in-house XPS and high energies (2000-7000 eV) correspond to hard X-ray PES (Bessy II synchrotron). The spectra display a first Si 2p peak (composed of $2p_{3/2}$ and $2p_{1/2}$ due to spin-orbit coupling) assigned to bulk silicon (~99.5 eV, in grey) and another one assigned to surface oxide (~103.5 eV, in red). The relative intensity of both peaks changes dramatically when the photon energy changes. Indeed, the increase of the photon energy results in an increase of the kinetic energy of the photoelectrons. Since the inelastic mean free path of the photoelectrons is highly dependent

on their kinetic energy [25] this leads to a significant change of the PES analysis depth. The silicon powder used in this work consists of ~50 nm mean diameter nanoparticles covered by a thin SiO_2 layer.

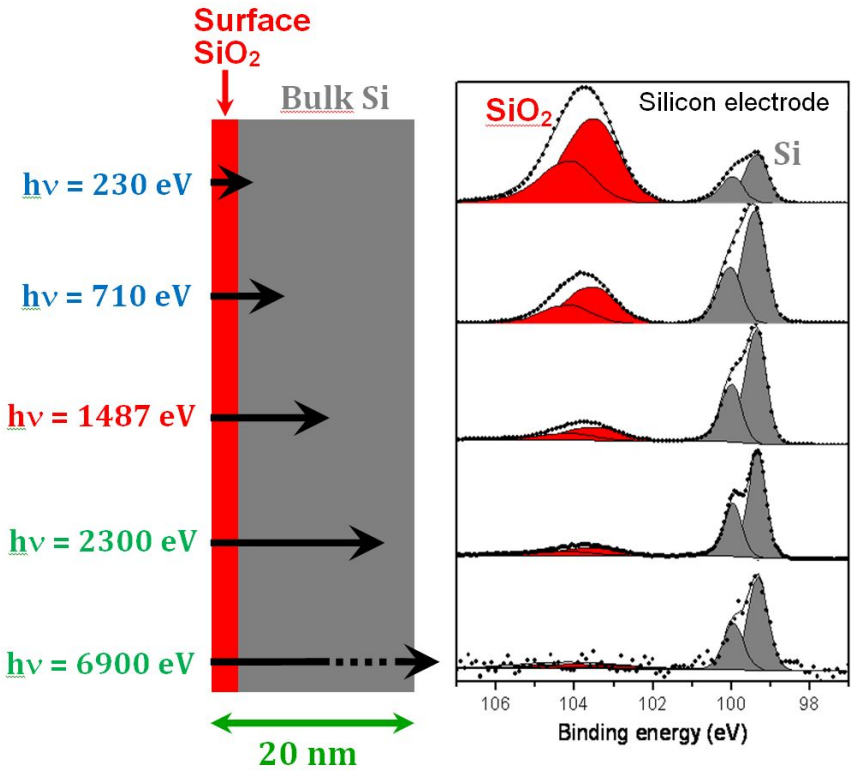

Figure 1: Influence of the photon energy on the Si 2p spectrum of the pristine silicon electrode. Schematic view of the evolution of the analysis depth (arrow) as a function of the photon energy hν.

As shown in figure 1, the variation of the photon energy allows thus to highlight the extreme surface of the particles or, at the opposite, to enhance the signal of the bulk. This experimental approach provides information about the repartition of species at the surface of the samples and avoids the argon-ion sputtering technique commonly used for depth-profiling, which is destructive for delicate surfaces such as those of Li-ion battery electrodes. Note that

the increase of the photon energy also results in a decrease of the PES cross-sections. Note finally that the SiO_2 oxide surface layer may be covalently bound to the CMC binder, as it was proposed by several authors to explain the efficiency of this binder [14,26]. However, it is rather difficult to evidence the existence of these bonds by XPS since it does not significantly modify the local environment of silicon.

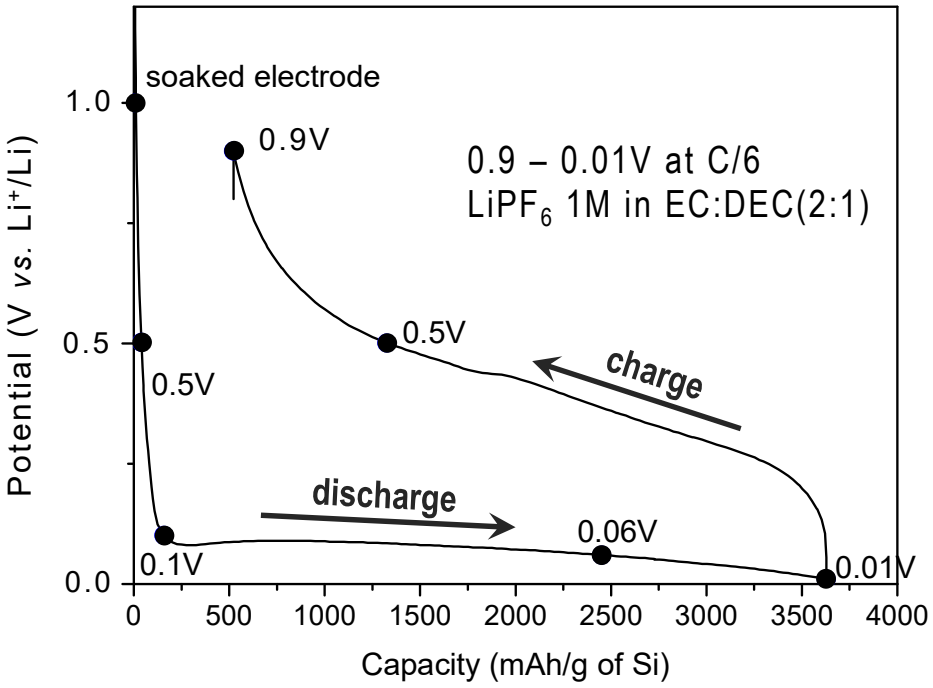

Figure 2: First discharge/charge cycle of the Si/C/CMC composite electrode *vs.* Li^0 cell between 0.01 and 0.9 V at C/6 rate. The samples analyzed by XPS are highlighted by black points.

Figure 2 shows the first galvanostatic discharge/charge cycle (between 0.01 and 0.9 V at C/6 rate) of an electrochemical cell built with the Si/C/CMC composite electrode *vs.* metallic lithium. This discharge/charge curve is in good agreement with previous results on nanosized

Si particles [15]. Upon full discharge about 3.8 moles of lithium are consumed per mole of silicon, corresponding to a discharge capacity of ~3650 mAh/g, and upon charge about 3.25 moles of lithium are restored, corresponding to an initial reversible capacity of ~3100 mAh/g. The electrochemical steps highlighted by black points correspond to the samples analyzed by PES.

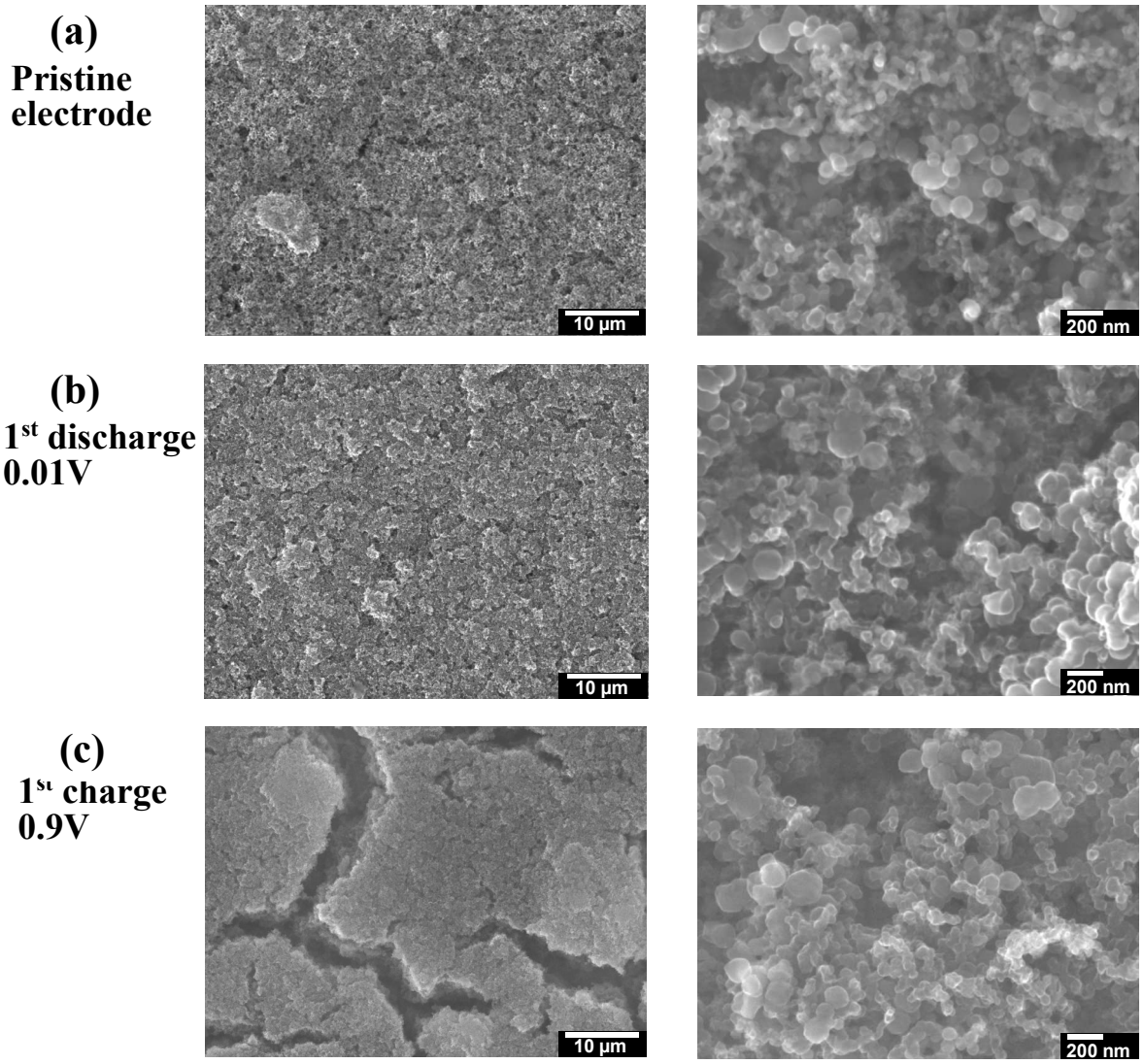

Figure 3: SEM images (10 µm and 200 nm scales, horizontal bars) of the Si/C/CMC composite electrode **(a)** pristine electrode, **(b)** after discharge at 0.01 V, **(c)** after charge at 0.9 V.

Scanning Electron Microscopy (SEM) images of Figure 3 show the morphological changes undergone by the composite electrode upon discharge and charge. These results are in good agreement with previous works [27]. Upon discharge, the reaction of silicon with lithium leads to a volume expansion of the particles, and the removal of this lithium upon charge results in the formation of cracks within the electrode. This is clearly seen in the 10 μm image after the first charge. As shown previously, these mechanical strains are partly responsible for the poor reversibility of silicon electrodes when discharged down to very low voltages *vs.* Li^+/Li [10].

3.1. Li-Si alloying process and silicon-containing surface phases:

Figure 4 shows the Si 2p spectra of the Si/C/CMC composite electrode upon the first discharge/charge cycle, and their dependence on the photon energy (hν), and thus on the analysis depth.

At the beginning of discharge (0.5 V), no changes can be seen with respect to the pristine electrode. The same Si 2p components can be observed. At this stage the reaction of lithium towards silicon has not yet started.

The first changes are observed after discharge at 0.1 V. Two additional components appear. The first one (Si $2p_{3/2}$ at 97.5 eV, yellow in Fig. 4) is attributed to a Li_xSi alloy. It shows that the formation of the Li-Si alloy has just started at the very beginning of the 0.1 V plateau. In the careful ^7Li NMR study of silicon electrodes reported by Key *et al.* [28], the authors have shown that the formation of the Li-Si alloy has not yet started at the exact starting point of the plateau (0.11 V in this case), but that it begins to take place between 0.11 and 0.105 V. This difference compared to our results can be explained by the fact that NMR probes the whole sample with a negligible contribution of the surface, especially for

micrometric samples. Our results show that the formation of the Li-Si alloy has just started at the surface of the particles at the very beginning of the 0.1 V plateau.

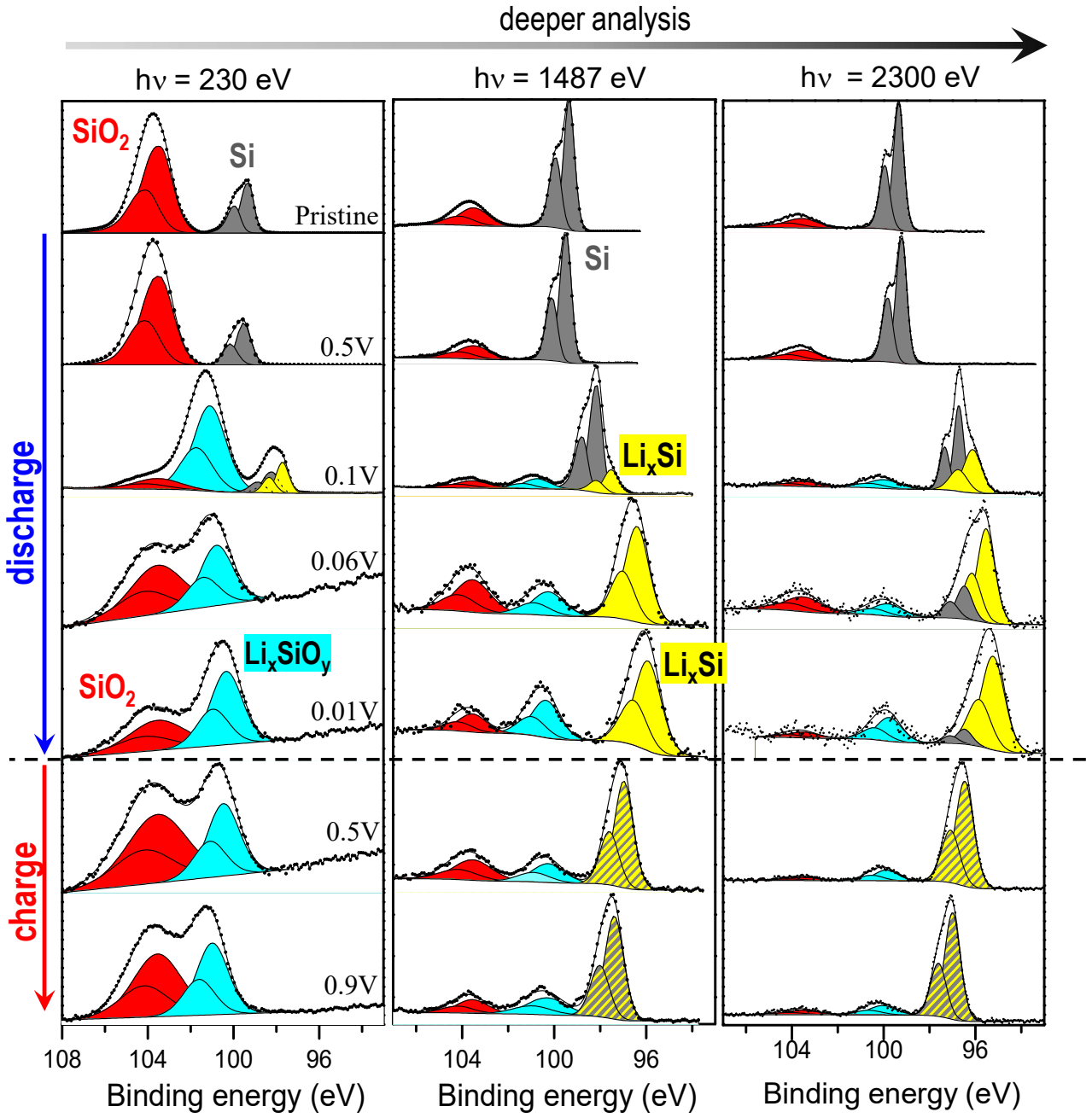

Figure 4: Si 2p spectra of the Si/C/CMC composite electrodes upon the first discharge/charge cycle (samples highlighted by black points in Fig. 2). Evolution as a function of the photon energy.

The second component appearing at 0.1 V (Si $2p_{3/2}$ at 100-101 eV, blue in Fig. 4) corresponds to an additional silicon-containing phase. Comparison of spectra obtained with three different photon energies (230, 1487 and 2300 eV) shows that its intensity has its maximum for the smallest analysis depth. It is thus located at the extreme surface of the particles. This surface phase most probably corresponds to Li_xSiO_y. Its chemical nature will be discussed later. In all the Si 2p spectra recorded at this stage, it is also possible to notice a shift of the component attributed to silicon (grey in Fig. 4) towards low binding energies. This shift could first be interpreted as the formation of another Li-Si alloy (with poorer lithium content). However, since no broadening of this component is observed with respect to the pristine silicon material, this shift would be rather explained by a differential charging effect. Indeed, during the XPS experiment, the emission of photoelectrons entails a loss of negative charge at the surface. For electronic conductors, this charge loss is easily balanced due to the electrical connection of the sample to a common ground with the spectrometer. However, when a sample is made up of mixed conducting and insulating compounds (like Li-ion battery electrodes) it is commonly observed that the signals of each type of compound are shifted differently (differential charging effect). Particularly, this is commonly observed when the surface of the sample is modified, when a passivation film forms at the surface for example [29,30]. The charging effect can partly be explained by a local charging due to poor conductivity in the insulating material. Therefore, the grey component is attributed to non-reacted silicon.

Upon further discharge (0.06 and 0.01 V *vs.* Li^+/Li), the Si 2p component assigned to silicon disappears, except for the largest analysis depth (2300 eV), which shows that the Li-Si alloying process is almost complete. The low voltage plateau corresponding to this stage is accompanied by an amorphisation process, as reported by previous works [8,31]. The Li_xSi component is gradually shifted to lower binding energies, which is probably due to the

increase of the lithium content x in Li_xSi, but may also be due to differential charging effect for this electronically conducting phase. Moreover, the Li_xSi alloy component cannot be observed when using the lowest analysis depth (230 eV), which shows again that the core of the particles is covered by a thin layer of SiO_2 and Li_xSiO_y phases. Note that the amount of SiO_2 seems to increase in the spectra from 0.1 to 0.06 V. However the total amount of silicon observed at the surface drops from 5.9 % to 0.9 % between these two steps and thus the amount of SiO_2 actually decreases.

After charging to 0.5 and 0.9 V *vs.* Li^+/Li, only small changes are observed concerning SiO_2 and Li_xSiO_y surface phases. A gradual increase of the binding energy of the component assigned to the Li-Si alloy is observed, that can be interpreted by a gradual decrease of the lithium content in the alloy. Contrary to discharge, no separate Li-Si and Si peaks are observed. This result is rather different from that obtained by Key *et al.* [32] from ^7Li NMR and X-ray pair distribution function analyses, who observed directly the formation of amorphous Si upon charge. However, this result certainly comes from a different behaviour of nanosized particles as compared to microsized particles, as already evidenced by electrochemical experiments. Indeed, these authors have worked with particles < 44 μm, while the particles size was ~50 nm in our case.

At the end of charge, an important broadening of the Li-Si alloy component is observed with respect to the pristine silicon material, despite most of the lithium has been extracted. This broadening may be due to the amorphisation process, or to a non-uniform lithium extraction due to the loss of electrical contact between some Si particles upon charge, as proposed by Oumellal *et al.* [33].

A part of this study has been devoted to the interpretation of the fourth component corresponding to the additional surface phase (100-101 eV, blue in Fig. 4). This component

could be first interpreted as coming from SiO_x or Li_xSiO_y phases. We analyzed "SiO" powder (Aldrich, < 44 µm) for comparison, but the Si 2p spectrum of this compound mainly revealed a mixture of SiO_2 and Si, with a negligible contribution of a third phase, the signature of which (101.8 eV) being rather far from that observed at the surface of our samples. Careful PES analyses of SiO_x layers forming at the SiO_2/Si interface have been carried out in previous works [34,35]. However, the Si 2p signature of these "SiO_x" species is always very weak with respect to SiO_2. Moreover the "SiO_x" signal most often consists of a gradual shift between several components assigned to Si^+, Si^{2+} and Si^{3+} oxidation states and with binding energies distributed over a region up to 4 eV from Si^{4+}. Instead, the appearance of the well resolved fourth component in Figure 4 appears as a consequence of the electrochemical lithium insertion and points to the presence of a Li_xSiO_y phase.

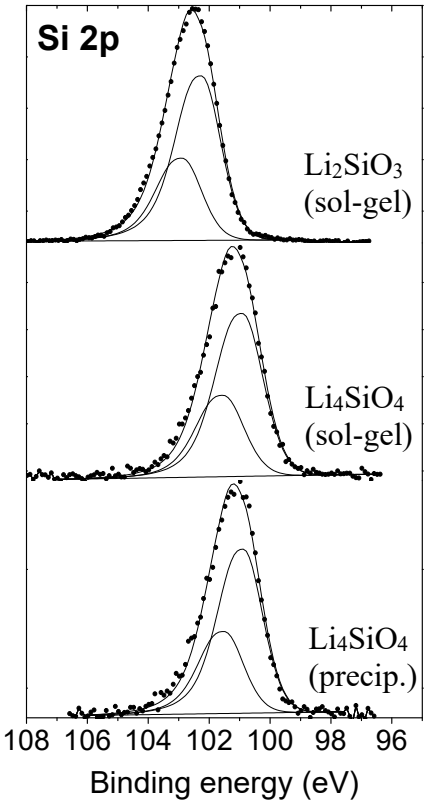

Figure 5: Si 2p spectra (in-house XPS, 1487 eV) of Li_xSiO_y compounds obtained from various synthesis attempts (sol-gel and precipitation methods).

Several synthesis attempts have been carried out in this work by sol-gel and precipitation methods to obtain various Li_xSiO_y phases described in the literature (see *Experimental details*). Synthesis attempts of Li_2SiO_3 and Li_4SiO_4 were successful. XPS Si 2p spectra of these compounds are plotted in figure 5. The observed Si $2p_{3/2}$ binding energies were 102.3 eV for Li_2SiO_3 and 100.9 eV for Li_4SiO_4. The value recorded for Li_4SiO_4 is very close to the additional component observed after electrochemical reaction with lithium. Therefore, we conclude Li_4SiO_4 is the most probable phase that appears at the surface of the silicon electrodes, although other mechanisms cannot be excluded. It is well known that the reaction of lithium with silicon leads to the reduction of the surface oxide according to the following reaction [36]: $SiO_2 + 4\ Li \rightarrow Si + 2\ Li_2O$. Our results on the electrochemical Li insertion point towards an additional mechanism occurring at the surface of the particles: $2\ SiO_2 + 4\ Li \rightarrow Si + Li_4SiO_4$. These conclusions are in good agreement with previous results obtained by Guo *et al.* [37] upon lithiation of nano-SiO_2 particles, or by Kim *et al.* [38] who showed from ^{29}Si and ^{7}Li NMR results the formation of Li_2O and Li_4SiO_4 upon reaction of lithium with "SiO", which was actually a mixture of Si and SiO_2.

Figure 6 shows O 1s spectra of the Si/C/CMC composite electrode upon the first discharge/charge cycle, and their evolution as a function of the analysis depth. The spectra of the pristine electrode show a maximum at 532.9 eV assigned to the CMC binder and to the surface oxide SiO_2 (same binding energy). After the beginning of the electrochemical reaction, a precise interpretation of O 1s spectra is more complex since many various oxygenated species are deposited at the surface of the electrode following the formation of the SEI, with specific signatures in a narrow binding energy range. However, it is possible to see that the maximum of the spectra shifts to lower binding energies (531.9-532 eV). This value is in good agreement with carbonates and organic species found in the SEI [39].

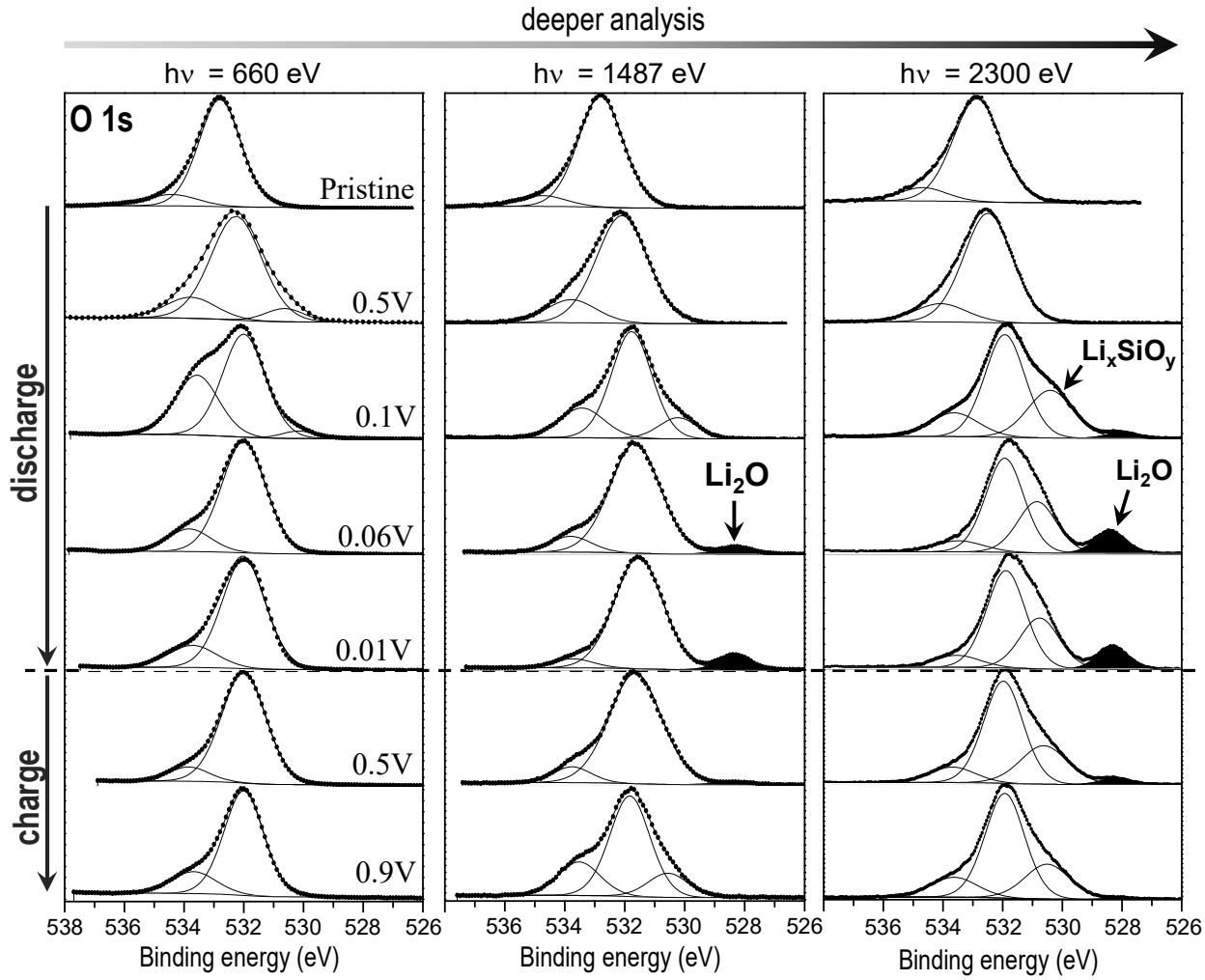

Figure 6: O 1s spectra of the Si/C/CMC composite electrodes upon the first discharge/charge cycle. Evolution as a function of the photon energy.

Due to its specific O 1s signature with a very low binding energy (528.4 eV), it is easy to detect Li_2O when it is formed at the surface of the silicon particle. As shown in Figure 6, Li_2O is detected only with the highest photon energies. Its intensity is highest for 2300 eV (and even higher for 6900 eV) which means that it is not located at the outermost surface of the samples, *i.e.* not in the SEI. For these highest photon energies, another O 1s component at

~530-530.5 eV can be also resolved, with a peak position in good agreement with the O 1s signature obtained for Li_4SiO_4. This shows that Li_2O and Li_4SiO_4 are the most buried oxygenated compounds in the samples, and this result allows us to position them at the interface between the SEI and the core silicon/Li_xSi particle. The reason why the O 1s signal of Li_4SiO_4 is more easily detected deep in the sample whereas its Si 2p signal is more easily detected at the surface is that the silicon electrode is covered by the SEI containing an important part of oxygenated species (resulting from degradation of the electrolyte) and no silicon-containing species. As a result, at the extreme surface of the sample the O 1s signal from the electrode material itself (and thus from Li_4SiO_4) is minority as compared to the whole O 1s signal mainly coming from other surface oxygenated species. The Li_4SiO_4 phase is thus located deeper in the sample than the other oxygenated species and its O 1s signal is more easily detected with higher photon energy (and so deeper analysis). On the other hand, since no silicon-containing species are present in the surface film, the SiO_2 and Li_4SiO_4 phases are located more at the surface of the sample than the other silicon-containing phases (*i.e.* Si and Li_xSi). Therefore, the Si 2p signal from these phases is more easily detected with lower photon energy (and thus more surface-sensitive analysis), but with a poor signal-to-noise ratio because the electrode is covered by the SEI. Another interesting result from O 1s spectra in Figure 6 is that the formation of Li_2O does not occur only at the beginning of discharge before the formation of the Li-Si alloy, but it takes place until the end of discharge. Moreover this mechanism with Li_2O formation is reversible upon the first cycle, since the O 1s signature of Li_2O gradually disappears upon charging.

3.2. Formation of the SEI:

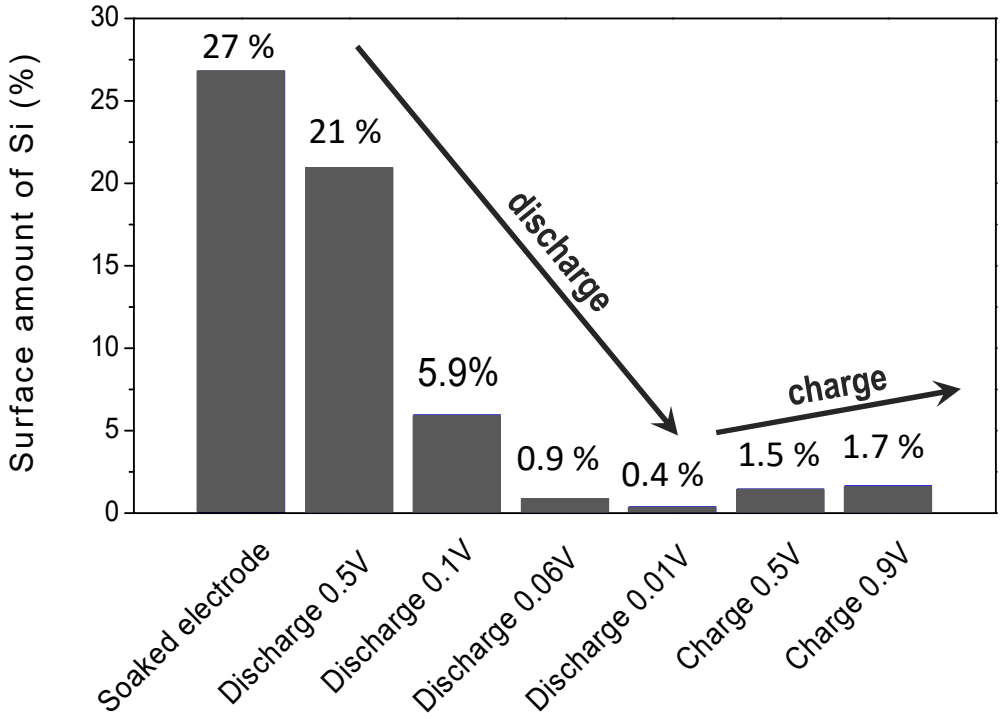

Figure 7: Evolution of silicon content at the surface of the electrodes determined from XPS spectra of the Si/C/CMC composite electrodes upon the first discharge/charge cycle (in-house XPS, 1487 eV).

Figure 7 shows the evolution of the total amount of silicon measured at the surface of the samples from Si 2p spectra upon the first cycle ($h\nu = 1487$ eV, analysis depth ~5-10 nm). Values are given as traditional atomic % although it is noted that such procedures are best suited for homogeneous materials. For a sample consisting of a bulk material (e.g. Si or Li-Si alloy) covered by a layer of different materials (e.g. the SEI) the variation of intensity is to a large extent the result from variations in attenuation. Therefore in the present study the atomic % reported in Figure 7 are mainly a measure of the increase (or decrease) of the thickness of the SEI. Here the figure shows a dramatic drop of the Si 2p signal upon discharge due to the formation of the SEI. Upon charge the Si 2p signal increases slightly, but remains

at very low values with respect to the non-cycled silicon electrode. This shows that the formation process of the SEI is mainly irreversible upon the first cycle.

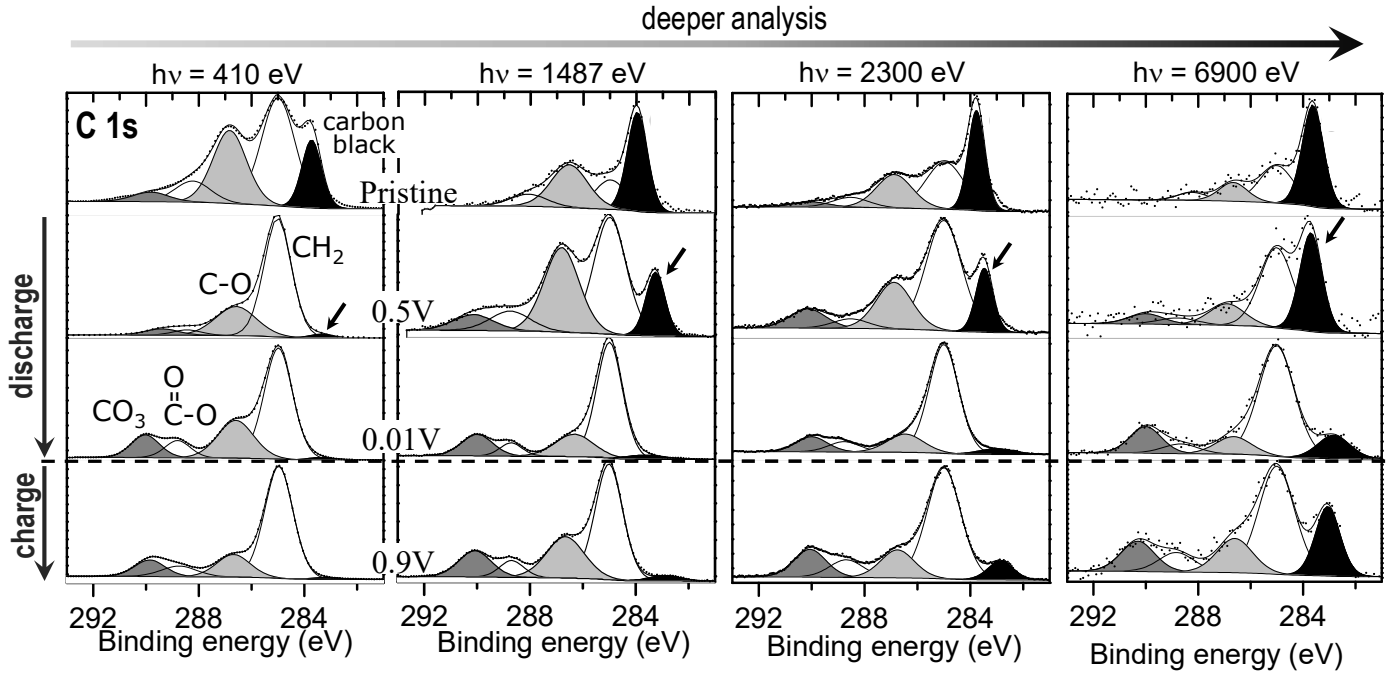

Figure 8: C 1s spectra of the Si/C/CMC composite electrodes upon the first discharge/charge cycle. Evolution as a function of the photon energy.

Figure 8 shows C 1s spectra of the Si/C/CMC composite electrode upon the first discharge/charge cycle, and their evolution as a function of the analysis depth. The spectra of the pristine electrode show several components, with relative intensities depending on the analysis depth. The narrow peak at ~284 eV (black in Fig. 8) corresponds to carbon black and it is much easier to observe this peak with greater analysis depths. The two peaks at ~286.5 and ~288.5 eV (grey and white, respectively) can be attributed to C-O and O=C-O

environments of carbon atoms in CMC binder, including carboxymethyl group. Finally the component at 285.0 eV (white) is assigned to hydrocarbon surface contamination.

At the beginning of discharge (0.5 V *vs.* Li^+/Li), the formation of the SEI has already started. The C 1s signal of carbon black can be hardly detected for the lowest analysis depth while it still remains observable for higher photon energies (indicated by an arrow). At the end of discharge (0.01 V *vs.* Li^+/Li), a thick SEI layer has formed and carbon black can be detected only at 2300 and 6900 eV. New carbonaceous species have been deposited at the surface, and their characteristic peaks corresponding to C-O (286.5 eV), O=C-O (288.5 eV) and CO_3 (290 eV) environments of carbon have gradually replaced the peaks of the pristine electrode. Particularly, carbonates (Li_2CO_3 and/or lithium alkyl carbonates) are present in the SEI. Note that the overall shape of C 1s spectra, and thus the composition of carbonaceous species, is similar to the composition of the SEI formed at the surface of graphite electrodes [40,41], or tin- and antimony-based intermetallic negative electrodes [29,42]. Several formation mechanisms of the species making up the SEI can be found in the literature [16,43,44,45]. After charge at 0.9 V, a slight re-increase of the carbon black signal reveals a slight decrease of the SEI thickness but a mainly irreversible SEI formation process, in good agreement with Si 2p signal shown above.

Two important features can be noticed in Figure 8. Firstly, by comparing the most surface sensitive and bulk sensitive modes we can see that at a given potential there is no major change in components of the C 1s spectra, and thus of the SEI constituents as a function of depth (as regards carbonaceous compounds). Second, at a given photon energy there is no major change in components of the C 1s spectra from the beginning of discharge (0.5 V) to the end of the first cycle (0.9 V). Some relative intensity fluctuations are observed but the general shape is similar. The same kind of observation could be done from O 1s spectra (some

small changes could be attributed to slight fluctuations of the amount of phosphates arising from degradation of the salt $LiPF_6$). This indicates that the overall composition of the SEI formed at the surface of the composite silicon electrodes is rather stable over the first discharge/charge cycle, and that only small fluctuations in composition over its thickness are observed. This is different from what is observed in the case of carbonaceous negative electrodes.

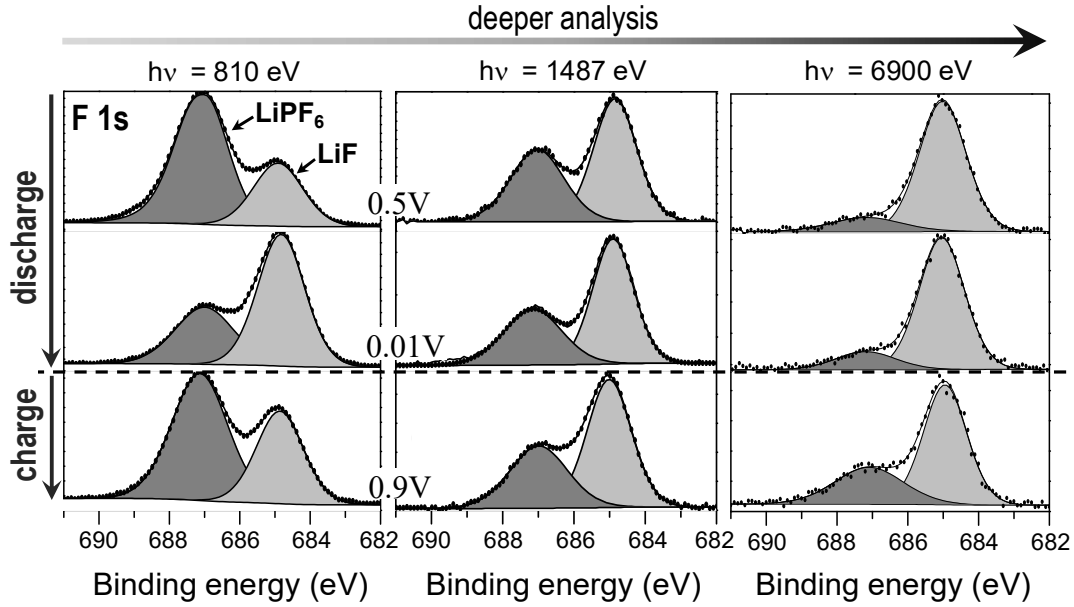

Figure 9: F 1s spectra of the Si/C/CMC composite electrodes upon the first discharge/charge cycle. Evolution as a function of the photon energy.

Additional information is provided by F 1s spectra of the same samples for different photon energies (Figure 9). The spectra show two components. The first one (~687 eV) is attributed to the salt $LiPF_6$ remaining at the surface of the electrodes, that was not dissolved by washing with the solvent DMC after battery opening. The second one (~685 eV) is

attributed to lithium fluoride LiF, which is one of the main degradation products of $LiPF_6$ (with phosphates). The figure shows at a given potential upon discharge or charge the relative intensity of $LiPF_6$ decreases as a function of the analysis depth. This indicates that the remaining traces of salt $LiPF_6$ are mainly located at the extreme surface of the SEI, while LiF is formed within the SEI layer.

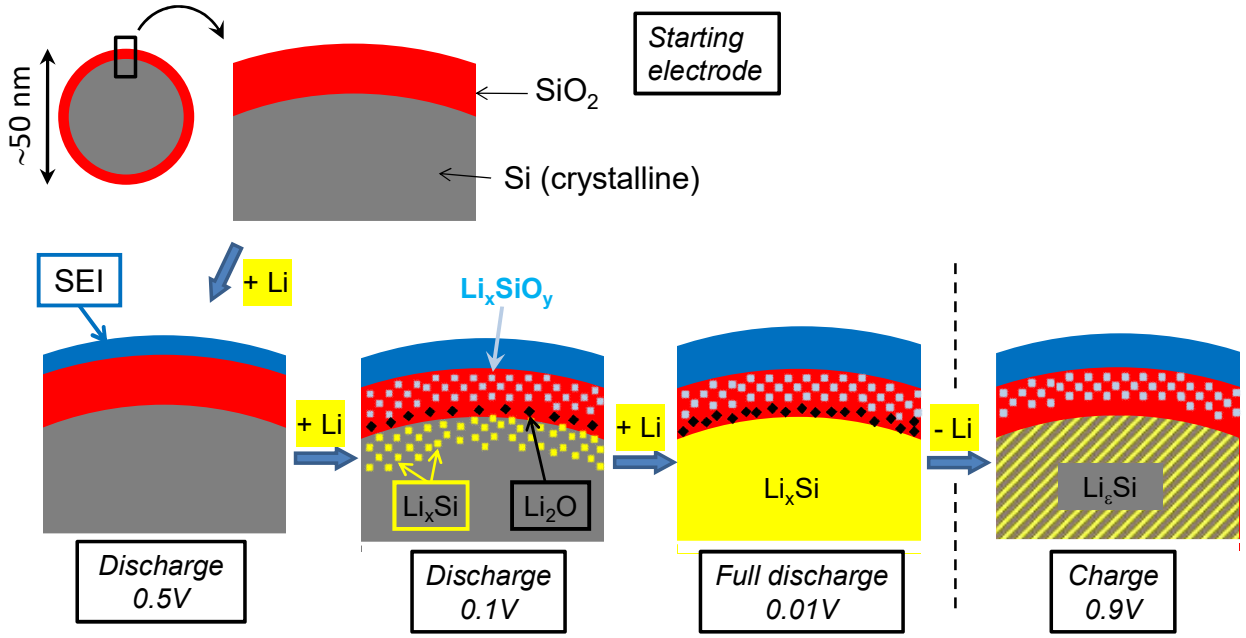

Figure 10: Schematic view of the mechanisms occurring at the surface of the silicon nanoparticles. Formation of the SEI at the beginning of discharge. Formation of the Li-Si alloy upon further discharge, together with Li_2O and Li_xSiO_y interfacial phases. Partial reversibility upon charge.

4. Conclusion

Figure 10 summarizes the observed results and provides a schematic view of the mechanisms occurring at the surface of the silicon nanoparticles upon discharge and charge. The pristine electrode consists of ~50 nm mean diameter nanoparticles covered by a thin SiO_2 layer. At the very beginning of discharge (0.5 V *vs.* Li^+/Li) lithium has not yet reacted with

silicon but a thin SEI layer has already formed. Its composition is very close to the SEI formed at the surface of carbonaceous electrodes, or Sn- or Sb-based intermetallics electrodes.

After further discharge, at the beginning of the low voltage plateau (0.1 V *vs.* Li^+/Li), the thickness of the SEI has increased, but its composition has not changed significantly. In the same time, lithium has started to react with the silicon nanoparticle. Reaction with the surface SiO_2 layer leads to the formation of Li_2O and Li_xSiO_y, most probably Li_4SiO_4. Reaction with the silicon leads to the formation of the Li-Si alloy. After full discharge (0.01 V *vs.* Li^+/Li), the Li-Si alloying process is almost complete, but some remaining unreacted silicon may be found in the core of the particle. The amount of Li_2O has increased continuously until the end of discharge, but some unreacted SiO_2 still remains at the surface. The thickness of the SEI has increased, but its composition has not changed significantly.

After full charge (0.9 V *vs.* Li^+/Li), lithium has been almost fully extracted from the core of the particle ($Li_\varepsilon Si$ with ε going down to zero). The thickness of the SEI has only slightly decreased, and Li_2O has disappeared.

By the originality of the experimental method (*i.e.* non-destructive depth-resolved XPS analysis by variation of the X-ray energy) and the new obtained results, this work opens the door to further investigations on the interfacial mechanisms of paramount importance in the field of Li-ion batteries.

Acknowledgements

This work was carried out in the framework of ALISTORE European Research Institute. The authors are grateful to the European Community for financial support. The authors are also grateful to the French Education and Research Ministry, and to StandUp for Energy, the Swedish Research Council VR and the Swedish Energy Agency.

References

[1] J. B. Goodenough and Y. Kim, *Chem. Mater.*, 2010, **22**, 587-603

[2] B. L. Ellis, K. T. Lee and L. F. Nazar, *Chem. Mater.*, 2010, **22**, 691-714

[3] J. W. Fergus, *J. Power Sources*, 2010, **195**, 939-954

[4] H. Li, Z. Wang, L. Chen and X. Huang, *Adv. Mater.*, 2009, **21**, 4593-4607

[5] R. A. Sharma and R. N. Seefurth, *J. Electrochem. Soc*., 1976, **123**, 1763-1768

[6] B. A. Boukamp, G. C. Lesh and R. A. Huggins, *J. Electrochem. Soc.*, 1981, **128**, 725-728

[7] C. J. Wen and R. A. Huggins, *J. Solid State Chem.*, 1981, **37**, 271-278

[8] M. N. Obrovac and L. Christensen, *Electrochem. Solid-State Lett.*, 2004, **7**, A93-A96

[9] J. H. Ryu, J. W. Kim, Y.-E. Sung, and S. M. Oh, *Electrochem. Solid-State Lett.* , 2004, **7**, A306-A309

[10] M. N. Obrovac, and L. J. Krause, *J. Electrochem. Soc.*, 2007, **154**, A103-A108

[11] J. Li, R. B. Lewis and J. R. Dahn, *Electrochem. Solid-State Lett.*, 2007, **10**, A17-A20

[12] D. Larcher, S. Beattie, M. Morcrette, K. Edström, J.-C. Jumas and J.-M. Tarascon, *J. Mater. Chem.*, 2007, **17**, 3759-3772

[13] W.-J. Zhang, *J. Power Sources*, 2011, **196**, 13-24, 2011

[14] B. Lestriez, S. Bahri, I. Sandu, L. Roue and D. Guyomard, *Electrochem. Commun.*, 2007, **9**, 2801-2806

[15] J.-S. Bridel, T. Azaïs, M. Morcrette, J.-M. Tarascon and D. Larcher, *Chem. Mater.*, 2010, **22**, 1229-1241

[16] E. Peled and D. Golodnitsky, in *Lithium-Ion Batteries: Solid-Electrolyte Interphase*, ed. P. B. Balbuena and Y. Wang, Imperial College Press, London, 2004

[17] M. Wachtler, J. O. Besenhard and M. Winter, *J. Power Sources*, 2001, **94**, 189-193

[18] C. K. Chan, R. Ruffo, S. S. Hong and Y. Cui, *J. Power Sources*, 2009, **189**, 1132-1140

[19] Y. M. Lee, J. Y. Lee, H.-T. Shim, J. K. Lee and J.-K. Park, *J. Electrochem. Soc.*, 2007, **154**, A515-A519

[20] B. Zhang, M Nieuwoudt and A. J. Easteal, *J. Am. Ceram. Soc.*, 2008, **91**, 1927-1932

[21] H. Pfeiffer, P. Bosch and S. Bulbulian, *J. Nucl. Mater.*, 1998, **257**, 309-317

[22] D. A. Shirley, *Phys. Rev. B*, 1972, **5**, 4709-4714

[23] J. H. Scofield, *J. Electron Spectrosc. Relat. Phenom.*, 1976, **8**, 129-137

[24] M. Gorgoi et al., *Nucl. Instrum. Methods Phys. Res. A*, 2009, **601**, 48-53

[25] M. P. Seah, *Surf. Interface Anal.*, 1986, **9**, 85-98

[26] N. S. Hochgatterer, M. R. Schweiger, S. Koller, P. R. Raimann, T. Wöhrle, C. Wurm and M. Winter, *Electrochem. Solid-State Lett.*, 2008, **11**, A76-A80

[27] L. Y. Beaulieu, K. W. Eberman, R. L. Turner, L. J. Krause and J. R. Dahn, *Electrochem. Solid-State Lett.*, 2001, **4**, A137-A140

[28] B. Key, R. Bhattacharyya, M. Morcrette, V. Seznec, J.-M. Tarascon and C. P. Grey, *J. Am. Chem. Soc.*, 2009, **131**, 9239-9249

[29] K. K. D. Ehinon, S. Naille, R. Dedryvère, P.-E. Lippens, J.-C. Jumas and D. Gonbeau, *Chem. Mater.*, 2008, **20**, 5388-5398

[30] R. Dedryvère, D. Foix, S. Franger, S. Patoux, L. Daniel and D. Gonbeau, *J. Phys. Chem. C*, 2010, **114**, 10999-11008

[31] T. D. Hatchard and J. R. Dahn, *J. Electrochem. Soc.*, 2004, **151**, A838-A842

[32] B. Key, M. Morcrette, J.-M. Tarascon and C. P. Grey, *J. Am. Chem. Soc.*, 2011, **133**, 503-512

[33] Y. Oumellal, N. Delpuech, D. Mazouzi, N. Dupré, J. Gaubicher, P. Moreau, P. Soudan, B. Lestriez and D. Guyomard, *J. Mater. Chem.*, 2011, **21**, 6201-6208

[34] F. J. Himpsel, F. R. McFeely, A. Taleb-Ibrahimi and J. A. Yarmoff, *Phys. Rev. B*, 1988, **38**, 6084-6096

[35] P. J. Grunthaner, M. H. Hecht, F. J. Grunthaner and N. M. Johnson, *J. Appl. Phys.*, 1987, **61**, 629-637

[36] J. Saint, M. Morcrette, D. Larcher, L. Laffont, S. Beattie, J.-P. Pérès, D. Talaga, M. Couzi and J.-M. Tarascon, *Adv. Funct. Mater.*, 2007, **17**, 1765-1774

[37] B. Guo, J. Shu, Z. Wang, H. Yang, L. Shi, Y. Liu and L. Chen, *Electrochem. Commun.*, 2008, **10**, 1876-1878

[38] T. Kim, S. Park and S. M. Oh, *J. Electrochem. Soc.*, 2007, **154**, A1112-A1117

[39] R. Dedryvère, L. Gireaud, S. Grugeon, S. Laruelle, J.-M. Tarascon and D. Gonbeau, *J. Phys. Chem. B*, 2005, **109**, 15868-15875

[40] A. M. Andersson, M. Herstedt, A. G. Bishop and K. Edström, *Electrochimica Acta*, 2002, **47**, 1885-1898

[41] R. Dedryvère, H. Martinez, S. Leroy, D. Lemordant, F. Bonhomme, P. Biensan and D. Gonbeau, *J. Power Sources*, 2007, **174**, 462-468

[42] M. Stjerndahl, H. Bryngelsson, T. Gustafsson, J. T. Vaughey, M. M. Thackeray and K. Edström, *Electrochimica Acta*, 2007, **52**, 4947-4955

[43] E. Peled, *J. Electrochem. Soc.*, 1979, **126**, 2047-2051

[44] D. Aurbach, M. L. Daroux, P. W. Faguy and E. Yeager, *J. Electrochem. Soc.*, 1987, **134**, 1611-1620

[45] A. M. Andersson and K. Edström, *J. Electrochem. Soc.*, 2001, **148**, A1100-A1109